CFD Study and Energy Optimization of Industrial Double-Cyclone in HDPE Drying Process

■

S.A. Razavi Alavi[1], E. Nemati Lay[2*]

■

[1] Department of Chemical Engineering, Faculty of Engineering, University of Kashan, Kashan, I.R.Iran
razavialavi@yahoo.com

[2] Department of Chemical Engineering, Faculty of Engineering, University of Kashan, Kashan, I.R.Iran
enemati@kashanu.ac.ir

■

Abstract

A double-cyclone is used as a gas-solid separator in the fluid bed-drying process to prepare dry HDPE powder from a wet feed rate of 56000 kg/hr. Particles' behavior and flow pattern in the dryer affect the cyclones as effective equipment. In evaluation of this system, the numerical simulation of the fluid flow field and particle dynamics, presented by CFD technique, characterize cyclone pressure drop and turbulence parameters. Navier-Stoke equations through the Euelerian-Lagrangian framework by RNG k-ε turbulence model are used as mathematical methods and the calculated results are in an acceptable agreement with industrial parameters. The obtained carrier gas flow rates of 14040, 14011 and 14000 m^3hr^{-1} as thermal energy for PE100, BL3, and EX5 respectively cause excellent flow regime, desired final volatile of 0.04%, 0.06% and 0.07% as well as high separation efficiency in different HDPE grades. The created flow pattern in the dryer makes the efficient use of the immersed coils as another source of energy for drying the particles. Double-cyclones conduct the minimum escaped contents of 70.2, 75.8 and 76.2 for the distributor section and 69.3, 75.3, 75.9 gr in 1 hr for the scrubbing tower. These rates of dusts provide the optimized electrical energy consumptions with maximum saving value of 17%.

Keywords: CFD, HDPE, Fluidized Bed Drying, Energy Optimization, Double-Cyclone, Pressure Drop.

---

* Corresponding Author

1. Introduction

Drying in the fluidized bed process is ideal for the heat-sensitive products like HDPE. Uniform operational conditions are established using the controlled speed of the carrier gas passing through the layer of the materials inside the dryer; this situation creates the fluidized state [1]. In the fluid bed drying, heat is provided by the hot carrier gas stream with or without additional heat transfer provided by immersed heat exchangers in the bed. Fluid bed drying offers significant advantages over other methods of particulate drying [2]. Actually, this operation offers the fluidizing of particles, an easy transfer of materials, and a high change rate of energy with required thermal efficiency along with preventing the extreme heating of particles individually [3]. The fluidizing gas passes through the distributor plate, and it is uniformly distributed across the bed to form a two-phase flow pattern of gas-particles. Characterizing the hydrodynamic behavior in fluidized bed is very complex and must be understood in improving the fluidization [2-5]. Operating parameters such as nitrogen velocity and pressure drop are used to understand the behavior of a material while it is fluidized [6]. At low gas velocities, the bed of particles rests on a gas distributor plate which shows the loss of fluidizing gas (N_2), and such loss results in collapse of the fluidized bed. Furthermore, illogical high velocity of nitrogen leads to generate phenomena such as 'elutriation' and 'carryover'. Accordingly, in a moving gas stream with a number of particles with a definite range of particle size, some particles may fall or rise depending on their size and positions. The best conditions will take place on the border between two phenomena of collapse and carryover, representing the proper hydrodynamic regime in the fluid bed system [3, 6-8]. Thus, the entrainment of particles in an upward-flowing gas stream is a complicated process. To achieve these optimal conditions, we need an efficient tool like the cyclone separators which are often used in the fluidized beds in order to separate entrained solids from the gas stream; they are installed within the fluidized bed vessel to show the behavior of flow field by the use of its pressure drop [3, 6]. Fluidized systems may have two or more stages of cyclone in series in order to improve separation efficiency as shown in Fig. 1 [6]. In the application of cyclones, tangential inlets are preferred due to the separation of solid particles from gases [9, 10].

On the other hand, in a novel design, David Winfield et al. [11] used triple inlet cyclone due to lower pressure drop with an approximately identical performance with the single inlet cyclone. A smaller inlet diameter leads to rotational flow velocities, reduced erosion rates in the cyclone body, and the maintenance of a stable vortex gas core [11]. Particles in the gas are subjected to centrifugal forces which move them radially outward, against an inward flow of gas and toward the inside surface of the cyclone on which the solids become separated [9, 12, 13]. It is obvious that the used force on the particles is a crucial factor determining the separation mechanism of a particle in the cyclone. Among several analyses of separation behaviors in the cyclones such as residence time [14], balanced orbital [15-17], and boundary layer theory [18, 19], the balanced orbital hypothesis is the most usable theory. Based on this theory, the force balance of a particle swirling on the interface between outer and inner vortices (as shown in Fig.2 [1]) plays a vital role.
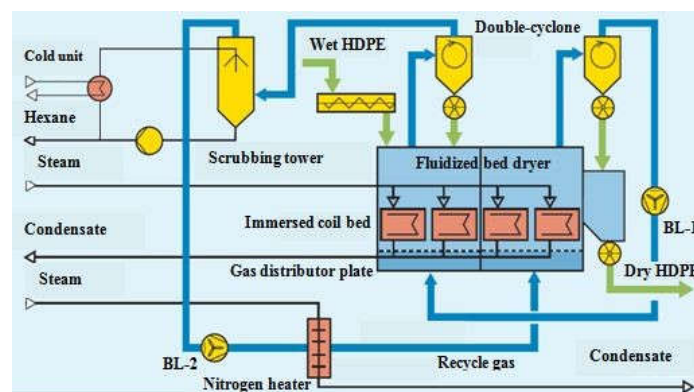
Fig. 1: Schematic of the fluidized bed drying system.

Theoretical studies do not completely explain the separation performance of cyclones; therefore, many experimental works and different ways have been investigated regarding this issue [20]. For instance, Ter Linden showed the complexity of separation mechanism through a spherical pitot tube [21]. Laser Doppler Anemometer (LDA) is also a developed method which revealed a rise in the velocity fluctuations caused by the contraction of the spigot [22]. The Precession Vortex Core (PVC), leading to undesired fluctuations in the internal swirl section, is an undesirable factor for the cyclone efficiency [23]. This impact as an unsteady-flow phenomenon essentially influences the movement of small particles like vortex core breakdown and natural turning length [24-26]. Accordingly, the behavior of the entrained particles is very important to characterize the separation process of cyclones. Solero and Coghe [20] proved the importance of the gas drag force in the particle motion by the use of LDA., there are three methods to evaluate particles' motions and their escape toward inner vortex. These ways are particle dynamic analyzer (PDA), positron-emission particle-tracking technology, and fiber optic detection used by Su and Mao, Chan et al. and Li et al. respectively [27-29]. Thus, it is clear that, the imposed forces on the particles, the flow field, and the separation efficiency are very effective in the study the particle separation mechanism [20]. In fluidization system, the factors affecting the rate of entrainment of solids from a fluidized bed are particle size distribution (PSD), terminal velocity, superficial gas velocity, particle density, and gas properties and gas flow regime [3, 30, 31]. Hence, it is necessary to understand gas-particle flow and the separation characteristics of the cyclone as a complementary unit in the drying process [3, 6]. Interestingly, the performance of the cyclone is determined using its pressure drop between input and output [1, 32, 33].

Computational Fluid Dynamics (CFD) as an alternative can accurately describe the flow field of the cyclone by turbulence models such as the Reynolds Stresses Model (RSM), Standard k-ε and RNG k-ε [34-37]. Eulerian-Eulerian and Eulerian-Lagrangian methods are two main approaches to simulate gas-solid flow [38]. In this regard, CFD method solves conservation equations of mass, momentum, and additional transport. In the turbulent flow, a set of nonlinear and partial differential equations like the continuity and Navier-Stokes that describe the fluid flows mathematically are solved [38, 39].
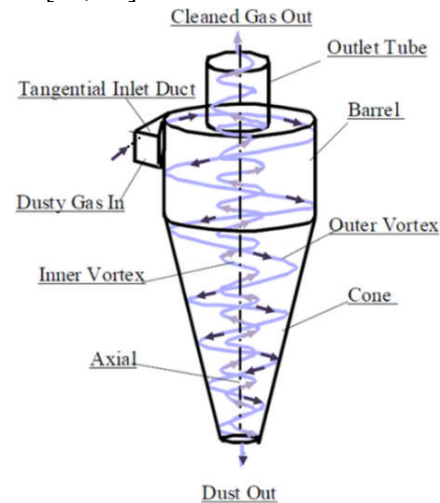
Fig. 2: Schematic diagram of a reverse flow cyclone separator [1]

Turbulence models based on statistical mechanics rather than continuum mechanics are mathematically simple. RNG-based k-ε model is derived using a statistical technique called renormalization group theory[40]. Substantially, the Lagrangian discrete phase is based partially on the physical properties of dust particles and partially on the mathematical modeling with certain reasonable assumptions which are considered to characterize the particles' transport in a fluid medium [41]. It is known that the pressure drop over a cyclone separator is the difference of static pressure between inlet and outlet. The static pressure at inlet cross-section is uniformly distributed because there is no swirling motion; hence, it can be easily measured with a pressure tapping on the wall [32]. In the past, Stairmand ignored the influence of the swirling flow; however, it was not precise. Shepherd and Lapple discharged the air directly from the cyclone to atmosphere, whereas the latter two ways have widely been used in experimental works and engineering fields [42, 43]. Essentially, the main part of the pressure drop about 80% is considered pressure losses inside the cyclone due to energy dissipation by the viscous stress of the turbulent rotational flow [44]. The remaining 20% of the pressure drop is caused by the contraction of the

fluid flow at the outlet and its expansion at the inlet as well as by fluid friction on the cyclone wall surface. Because of strong swirling flow at the outlet pipe, the static pressure measurement becomes complicated and difficult sinceit necessitates the utilization of CFD modeling of the cyclones [11, 20, 32, 45]. Accordingly, numerous CFD simulations have successfully been applied by employing different mathematic models to determine the features of gas-solid flow field for the cyclones [46-52]. Moreover, Houben et al. used RSM and k-ε model to simulate pressure drop and velocity field in a cyclone [53].

To date, many investigations have mainly focused on the study of the cyclones as independent gas-solid separation units. However, this paper accurately presents an analysis of double-cyclones as a complementary section in the fluid bed drying process. Actually, as a novel idea, we consider this equipment as a section which reflects operating behaviors of the drying system through industrial-CFD experiments. Required operating gas flow rate and proper cyclone pressure drop are calculated in various HDPE grades including PE100, BL3 and EX5. Furthermore, these obtained results are assessed by both evaluating energy consumption of all of the employed blowers and monitoring the dust content for the final destination of the cyclone gas outlet. Based on previous experiments, it becomes clear that the short-circuit flow, the re-entrainment (including the reverse gas stream from the dust duct) and the drag force toward the inner vortex area affect the escape of the particles [54]. Hence, the CFD results combined with the electrical energy consumptions of blowers with respect to the captured dust contents helps improve the cyclone performance in various operating conditions.

2. Industrial Experiments
2.1. Experimental Material

Normal hexane as the liquid content of the polymer; nitrogen (as dry gas carrier); water steam for heating the coils within the drying bed; and different grades of high density polyethylene such as PE100, BL3 and EX5 as bimodal polymers are the materials used in our research. Their details are reported in Tables 1 and 2.

Table 1: Physical specifications of experimental materials

Descriptions	Values
Nitrogen (N_2)	
ρ_g (kg m^{-3})	1.251
μ_g (kg m^{-1}s^{-1})	2.07×10^{-5}
Normal hexane (HX)	
ρ_l (kg m^{-3})	659
μ_l (kg m^{-1}s^{-1})	3×10^{-4}
HDPE-PE100 (based on ZN -1)	
ρ_p (kg m^{-3})	948 ± 0.002
ρ_{Bp} (kg m^{-3})	450
HDPE-BL3 (based on ZN -2)	
ρ_p (kg m^{-3})	953 ± 0.002
ρ_{Bp} (kg m^{-3})	392
HDPE-EX5 (based on ZN -2)	
ρ_p (kg m^{-3})	948 ± 0.002
ρ_{Bp} (kg m^{-3})	396

Table 2: Particle size distribution for PE100, BL3 and EX5 respectively as HDPE grades

Size (μm)	volume (%)	volume (%)	volume (%)
450.00	2.92	0.68	0.28
357.50	7.80	1.44	1.32
282.50	6.56	0.04	0.76
225.00	30.04	8.80	11.36
180.00	24.36	28.00	25.64
142.50	16.32	34.12	27.76
94.00	5.32	24.92	29.28
63.00	3.28	1.84	3.12

2.2. Experimental Equipment

Based on Fig.3, the experimental-industrial system includes drying duct with two beds, immersed coil bed, nitrogen heater, nitrogen distribution plate, gas blowers (BL-1,2), scrubbing tower, double-cyclone (CY-1,2), rotary valves (BW-1,2), pressure gauges (PI-1,2), differential pressure gauges (PDI-1,2,3,4,5,6,7), temperature gauges (TI-1,2,3,4,5,6,7,8,9,10,11,12,13), and flow meter (FI-1,2) which all consist the investigated fluidized bed drying system.

2.3. Experimental Method

In this work, after ethylene polymerizing, HDPE as a suspension is received by a receiver tank which contained 1 ton of the polymeric powder per about 4-5 m^3 of hexane. This large quantity of diluents has to be removed before pelletizing the powder. Centrifugal step and fluid bed dryer will help separate solvent from the polymer, so hexane separation is commonly carried out using three centrifugal sections which are present to guarantee a total throughput of 40 t/h. In this system,

polyethylene-suspension will be pre-dried to approximately 20-30 % of residual hexane by centrifugal operation after receiver tank. The pre-dried product reaches the second stage where final drying will be applied to the required hexane content of 0.1%. The hot exhaust gas of the second drying stage with a temperature of approximately 78-80°C is de-dusted in CY-2 before being recompressed in BL-1 to be used to flash-dry the wet HDPE which comes in the first drying stage to about 1% hexane content (dry basis). Because of the high dust content of the drying gas, the gas distributor has a special slotted plate.
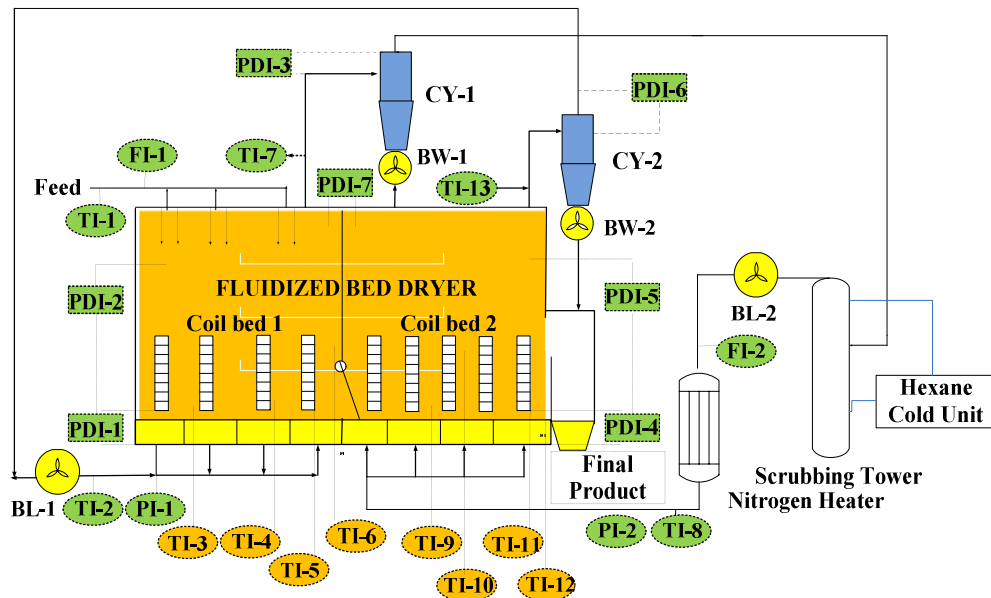
Fig. 3. Schematic of the experimental-industrial system

The nitrogen gas which is re-circulated from the second stage is simultaneously loaded with additional hexane which corresponds to about 35% relative humidity. The rich gas leaves the first drying stage at approximately 60°C to be de-dusted in CY-1; then, the gas must be regenerated by condensing the hexane that has been evaporated in the dryer using a scrubber tower. High dust loadings can be obtained through the process in which the double-cyclones help separate the entrained dried particles from the gas leaving the dryer [3, 10]. The performance of the system is indicated using the controlling devices installed on the feed flow rate, the volumetric gas flow rate, the pressure drop of the bed, and the cyclones and the amount of escaped particles from the cyclones. In addition,, the electrical energy consumptions and the monitoring of the dust content are evaluated by the aforementioned tests.

Changing the operating parameters to understand HDPE fluidized bed-drying process will yields results which can be seen in Tables 3 to 7. We examine different nitrogen flow rates (leading to various tangential velocities toward the double-cyclones) for powders with densities and PSDs shown in Tables 1 and 2. In the present experiments, due to the collapse and carry-over phenomena mentioned in the introduction section, we should strongly consider that the selected range of nitrogen (dry gas carrier) flow rates is not so vast. In the wet cake rate of 38000 kg hr $^{-1}$ and various gas flow rates (FI-2) of 14040, 14011 and 14000 m^{3}hr^{-1}, the first bed pressure drops at stable values of 3.239, 3.018, and 3.016 kpa which are resulted in PDI-2 for PE100, BL3 and EX5, respectively.

For the assessment of the performance of the double-cyclones and of their role in controlling the fluid bed drying, the proper gas flow rates in the drying system are determined to achieve the operating parameters listed in Tables 3 to 5. Besides, for completing our experiments, energy consumptions and elutriated powders are reported in Table 6 at suitable operating nitrogen flow rates.

Table 3: Operating parameters obtained in FI-2 of 14040 for PE100 grade			
Descriptions	**Values**	**Descriptions**	**Values**
FI-1(kg hr^{-1})	38000	TI-1(°C)	32.00
FI-2(m^{3}hr^{-1})	14040	TI-2(°C)	87.00
PI-1(kpa)	19.65705	TI-3(°C)	59.00
PDI-1(kpa)	1.01987	TI-4(°C)	62.20
PDI-2(kpa)	3.23995	TI-5(°C)	62.00
PDI-3(kpa)	2.0375	TI-6(°C)	63.20
PI-2(kpa)	19.65705	TI-7(°C)	60.00
PDI-4(kpa)	1.12915	TI-8(°C)	98.00
PDI-5(kpa)	3.2424	TI-9(°C)	86.80
PDI-6(kpa)	1.2159	TI-10(°C)	84.60
PDI-7(kpa)	0.101325	TI-11(°C)	87.00
Volatile(%)	0.04	TI-12(°C)	86.30
		TI-13(°C)	84.00

In the tests, for the evaluation of the hydrodynamic behavior of the drying system and the double-cyclones performance through different nitrogen flow rates in three HDPE grades, energy consumption of blowers is represented by KWI-1/2 and the captured particle contents in S.C-1/2 are shown in Table 7. In this paper, these listed values represent the influence of energy consumption methods and monitoring of the escaped particles.

Table 4. Operating parameters obtained in FI-2 of 14011 for BL3 grade			
Descriptions	**Values**	**Descriptions**	**Values**
FI-1(kg hr^{-1})	38000	TI-1(°C)	32.00
FI-2(m^{3}hr^{-1})	14011	TI-2(°C)	83.00
PI-1(kpa)	19.59711	TI-3(°C)	58.00
PDI-1(kpa)	1.03887	TI-4(°C)	61.90
PDI-2(kpa)	3.01812	TI-5(°C)	62.00
PDI-3(kpa)	2.0175	TI-6(°C)	63.00
PI-2(kpa)	19.61702	TI-7(°C)	59.00
PDI-4(kpa)	1.13815	TI-8(°C)	98.00
PDI-5(kpa)	3.1124	TI-9(°C)	85.40
PDI-6(kpa)	1.2149	TI-10(°C)	83.90
PDI-7(kpa)	0.101325	TI-11(°C)	86.00
Volatile(%)	0.06	TI-12(°C)	85.10
		TI-13(°C)	80.00

Table 5. Operating parameters obtained in FI-2 of 14000 for EX5 grade			
Descriptions	**Values**	**Descriptions**	**Values**
FI-1 (kg hr^{-1})	38000	TI-1(°C)	32.00
FI-2 (m^{3}hr^{-1})	14000	TI-2(°C)	83.00
PI-1(kpa)	19.59401	TI-3(°C)	57.00
PDI-1(kpa)	1.04981	TI-4(°C)	61.40
PDI-2(kpa)	3.01612	TI-5(°C)	61.80
PDI-3(kpa)	2.0045	TI-6(°C)	62.80
PI-2(kpa)	19.60522	TI-7(°C)	59.00
PDI-4(kpa)	1.14725	TI-8(°C)	98.00
PDI-5(kpa)	3.0154	TI-9(°C)	85.00
PDI-6(kpa)	1.2029	TI-10(°C)	83.10
PDI-7(kpa)	0.100895	TI-11(°C)	86.00
Volatile(%)	0.07	TI-12(°C)	84.70
		TI-13(°C)	80.00

Table 6. Optimized energy consumption of the blowers and the escape content of the dust					
HDPE grade	**FI-2 (m^3/hr)**	**KWI-1 (kw)**	**S.C-2 (gr of dust at 1 hr)**	**KWI-2 (kw)**	**S.C-1 (gr of dust at 1 hr)**
PE100	14040	58.52	70.20	99.27	69.30
BL3	14011	59.75	75.80	98.66	75.30
EX5	14000	59.81	76.20	98.04	75.90

Table 7. Energy consumption values of the blowers and the escape content of the dust					
HDPE grade	**FI-2 (m^3/hr)**	**KWI-1 (kw)**	**S.C-2 (gr of dust at 1 hr)**	**KWI-2 (kw)**	**S.C-1 (gr of dust at 1 hr)**
PE100	14070	59.75	75.50	99.89	70.90
PE100	14100	64.63	84.40	100.50	74.30
PE100	14130	68.28	90.60	101.12	75.90
BL3	14041	61.73	82.20	99.36	78.90
BL3	14071	66.96	91.30	100.10	84.30
BL3	14101	69.98	97.30	100.91	87.20
EX5	14030	61.62	82.30	98.74	79.00
EX5	14060	66.98	91.50	99.48	84.90
EX5	14090	68.75	96.80	100.31	86.70

3. Numerical Simulation Methods

3.1. Grid Division

The double-cyclones consist of a spiral hood, a cylinder body, and a cone and triangular dust hopper. At the bottom of the dust hopper, the rotary valves BW-1/2 prevent from the return of secondary gas streams from the pressurized dryer to the dust hopper. It, also, controls the dust flow rate from the hoppers to the dryer.

The geometrical dimensions of the cyclone separator used for the simulation are depicted in Table 8. Solid Works is a solid modeling computer-aided design (CAD) and a computer-aided engineering (CAE) program which is used as a 3D CAD software to quickly create and adjust 3D model geometry using direct model editing. This software is used in creating the sketch entities and geometry as a construction geometry of the cyclone that are ultimately incorporated into a section.

Table 8: The dimensions of the industrial double- cyclone

Geometric Data	Values
Cyclone diameter, D (mm)	1200
Inlet hieght, a(mm)	701
Inlet width, b(mm)	317
Cylinder hieght, H(mm)	2100
Cone hieght, h(mm)	1800
Gas outlet diameter, D_e (mm)	707
Dust outlet diameter, B (mm)	630
Gas outlet duct lengths, S (mm)	900

Figure 4 schematically illustrates the industrial double-cyclone geometry, dimensions, and grid arrangement. After importing previously generated CAD/CAE file into the meshable sections of Gambit software, the cyclone is meshed by tetra-hedral grids and divided by the coarse, moderate, and fine grids respectively. Based on the grid division, the final computational domain is divided finally by an unstructured grid, containing 370000 control mesh cells. Compared to the structured meshes, the storage requirements for an unstructured mesh can be substantially larger since the neighborhood connectivity must be explicitly stored. Meshing is an integral part of the CAE analysis process. Accordingly, the applied mesh influences the accuracy, convergence, and t speed of the solution, and the created geometry can be fitted with the unstructured tetra-hedral elements [55, 56].
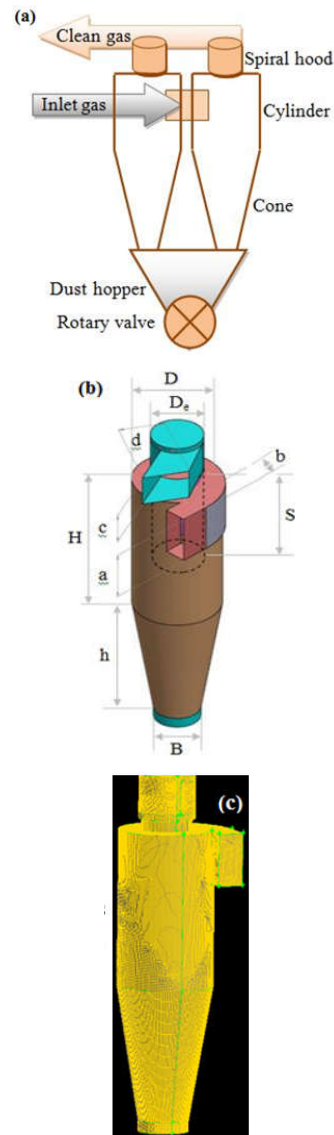
Fig. 4: a) Geometry of industrial cyclone b) Dimensions of the cyclone c) Computational grid used in the simulation

3.2. Modeling of the Fluid Flow

Based on the recent progress of computational power and numerical techniques, CFD has widely been applied in the industrial flow problems in the cyclone. The cyclone performance parameters such as pressure field, pressure drop, and turbulence parameters are governed by many operational parameters (e.g., the gas flow rate and particle properties) and geometrical parameters. This study focuses on the performance of the double-cyclone separator using ANSYS Fluent 15.0 with commercial finite volume solver by windows 7, 64 bit OS, 8 calculating core and 16 GB Ram. Usually, the fluid flows are mathematically described by a set of nonlinear and partial differential equations named

continuity and the Reynolds-averaged Navier-Stokes (RANS), which for the steady and incompressible fluid flow in the double-cyclone [57], the equations can be expressed as:

$$\rho u_j \frac{\partial u_i}{\partial x_j} = -\frac{\partial P}{\partial x_i} + \frac{\partial}{\partial x_j}\left[\mu\left(\frac{\partial u_i}{\partial x_j} + \frac{\partial u_j}{\partial x_i}\right)\right] + \frac{\partial \tau_{ij}}{\partial x_j} \qquad (1)$$

$$\tau_{ij} = -\rho \overline{\acute{u}_i \acute{u}_j} \qquad (2)$$

Where u, p, ρ, and μ represent fluid velocity, pressure, density, and viscosity respectively. And is defined as the Reynolds stress tensor, which represents the effects of turbulent fluctuations on the fluid flow in the cyclone.

$$\frac{\partial u_i}{\partial x_i} = 0 \qquad (3)$$

Is the continuity equation for the mean motion. However, the turbulence model should be used to determine the Reynolds stress tensor in the above equations. Moreover, in the modeling of the confined swirling flow, it is necessary to describe the turbulent behavior of the flow accurately. In this study, the RNG k-ε model is derived using a statistical technique named renormalization group theory, which is selected for calculating the flow field in the cyclone [34, 58, 59]. Transport equations for turbulent kinetic energy (k) and dissipation rate(ε) in the model, which are derived from Navier-Stokes equations using the renormalization group theory [60], can be presented as:

$$\rho \frac{Dk}{Dt} = \frac{\partial}{\partial x_i}\left(\alpha_k \mu_{eff} \frac{\partial k}{\partial x_i}\right) + G_k - \rho\varepsilon \qquad (4)$$

$$\rho \frac{D\varepsilon}{Dt} = \frac{\partial}{\partial x_i}\left(\alpha_\varepsilon \mu_{eff} \frac{\partial \varepsilon}{\partial x_i}\right) + C_{1\varepsilon}\frac{\varepsilon}{k}G_k - C_{2\varepsilon}\rho\frac{\varepsilon^2}{k} - R \qquad (5)$$

In these equations, G_k represents the generation of turbulence kinetic energy due to the mean velocity gradients, the constants $C_{1\varepsilon}$ and $C_{2\varepsilon}$ are assumed to be 1.42 and 1.68 respectively, and α_k and α_ε are the inverse effective Prandtl numbers for k and ε, respectively. Unlike k-ε standard model, this model includes an additional term (R) in its ε equation, which includes the effect of swirl on turbulence and an analytical formula for turbulent Prandtl number.

Based on the assumptions of governing equations, the transport equations of RSM can be written as following:

$$\frac{\partial}{\partial x_k}(\rho u_k \overline{\acute{u}_i \acute{u}_j}) = -\frac{\partial}{\partial x_k}\left(\frac{\mu_t}{\sigma_k}\frac{\partial \overline{\acute{u}_i \acute{u}_j}}{\partial x_k}\right) -$$
$$\rho\left(\overline{\acute{u}_i \acute{u}_k}\frac{\partial u_j}{\partial x_k} + \overline{\acute{u}_j \acute{u}_k}\frac{\partial u_i}{\partial x_k}\right) + p\overline{\left(\frac{\partial \acute{u}_i}{\partial x_j} + \frac{\partial \acute{u}_j}{\partial x_i}\right)} - 2\mu\overline{\frac{\partial \acute{u}_i}{\partial x_k}\frac{\partial \acute{u}_j}{\partial x_k}} \qquad (6)$$

The effective viscosity, μ_{eff}, is defined by:

$$\mu_{eff} = \mu + \mu_t \qquad (7)$$

Where μ_t is the turbulent viscosity as mentioned earlier. In the high-Reynolds number, Eq. (8) can be written as:

$$\mu_t = \rho C_\mu \frac{k^2}{\varepsilon} \qquad (8)$$

With C_μ=0.0845, it is derived using RNG theory. It is notable that the value of C_μ is very close to the empirically-determined value of 0.09 has been used in the standard k-ε model.

3.3. Modeling for the Particle Dynamics

In the fundamental mathematical modeling of two-phase flow, Lagrangian trajectory approach is widely used for simulating the particle flow in the cyclone. The Lagrangian method without consideration of the particle interactions, which is also called discrete phase model (DPM), is used to track individual particles through the continuum fluid [61]. The particle tracking method is used to model the dynamics of the particle which may be treated individually in the double-cyclone. One of the advantages of using the Lagrangian approach is the capability to easily alter the physical properties of individual particles such as diameter, density, etc.. Thus, based on Table1 and 2, this method will be proper for a double-cyclone simulation in different PSDs and densities of particles. Furthermore, local physical phenomena related to the particle flow behaviors can be easily probed. Accordingly, the Lagrangian model can also be used for the validation, testing, and development of continuum models [34, 50]. CFD method predicts the trajectory of a discrete phase particle by integrating the force balance on the particle written in a Lagrangian frame and the particle force balance relations in x, y and z directions respectively. This can be written as [59, 60]:

$$\frac{du_p}{dt} = F_D(u - u_p) + \frac{v_p^2}{r_0} \qquad (9)$$

$$\frac{dv_p}{dt} = F_D(v - v_p) - \frac{u_p v_p}{r_0} \qquad (10)$$

$$\frac{dw_p}{dt} = F_D(w - w_p) - g \qquad (11)$$

Where $\frac{v_p^2}{r_0}$ and $\frac{u_p v_p}{r_0}$ represent centrifugal and coriolis components of particle acceleration, respectively. In

above equations, $F_D(u - u_p)$ is the drag force per unit particle mass, and F_D can be expressed as:

$$F_D = \frac{18\mu}{\rho_p d_p^2} \frac{C_D Re}{24} \tag{12}$$

Where u is the fluid phase velocity; u_p is the particle velocity; μ is the molecular viscosity of the fluid; ρ is the fluid density; ρ_p is the density of the particle, and d_p is the particle diameter. Re is the relative Reynolds number, which is defined as

$$Re = \frac{\rho d_p |u_p - u|}{\mu} \tag{13}$$

The drag coefficient can be calculated as:

$$C_D = a_1 + \frac{a_2}{Re} + \frac{a_3}{Re^2} \tag{14}$$

Where a_1, a_2, and a_3 are the constants that are applied to smooth spherical particles over several ranges of Re as given by Morsi and Alexander [61].

3.4. Solution Algorithm

Pressure-velocity coupling is achieved via the Pressure-Implicit with Splitting of Operators (PISO) method, which is used as a solution technique in the cyclone CFD simulation. PISO scheme, as a part of the SIMPLE algorithms subcategory, is based on the approximate relation between the corrections of pressure and velocity. After the pressure correction equation is solved, new velocities and corresponding fluxes will not satisfy the momentum balance. Therefore, because of these limitations in the SIMPLE and SIMPLEC schemes, the PISO algorithm performs two additional corrections: a neighbor correction and a skewness correction for improving the efficiency of numerical simulation by repeating the calculation until the balance is satisfied [38, 39, 62, 63].

3.5. Boundary and Convergence Conditions

In the CFD investigation of double-cyclone, it is necessary to specify the boundary conditions at the inlet, outlet, and at the walls. Thus, pressure inlet boundary condition is applied at inlet; pressure outlet at gas outlet; and also wall (no-slip) boundary condition is used at all other boundaries. Moreover, in the particle phase conditions, in order to calculate the trajectories of the particles, it is necessary to provide required information regarding the starting position and the physical state of the particle. The physical state of t particles includes normally starting velocity, density, and size. Particle size distribution (PSD) can be defined by the Rosin-Rammler equation [33, 38]. The Rosin-Rammler distribution function is based on an assumption that an exponential relationship exists between the particle diameter (d) and the mass fraction of particles with diameter greater than d (Y_d):

$$Y_d = e^{-(d/\bar{d})^n} \tag{15}$$

CFD way refers to the quantity of d in Equation (15) as the mean diameter and to n as the spread parameter. These parameters have been created to define the Rosin-Rammler size distribution. Hence, the present experimental particle size distribution of HDPE, as shown in Table 2, is fitted in the Rosin-Rammler exponential equation. Finally, run calculation accomplished by the time stepping method, which is adjusted in the fixed stages with step size of 0.005 s and number of time step of 1200.

3.6. Simulated Results

3.6.1 Pressure Field in the Double-cyclone

Fig. 5 demonstrates a3D map that is a predicted static pressure profile of three polymer grades with different dry gas carrier (N_2) flows, densities, and particle size distributions. Nitrogen flow rate affect the pressure field in which the lowest pressure is located at the axis. Previous experiments have showed that the inlet flow rate is an effective parameter on the vortices in the cyclones, and unsuitable rate of it causes a negative pressure field. However, the present CFD results without a negative pressure field refer to 14040, 14011, and 14000 $m^3 hr^{-1}$ as fit values for PE100, BL3 and EX5 respectively. Moreover, a better symmetry and coincidence for the pressure field and the proper pressure gradient along radial direction are occurred in the double-cyclone through these defined operating parameters.
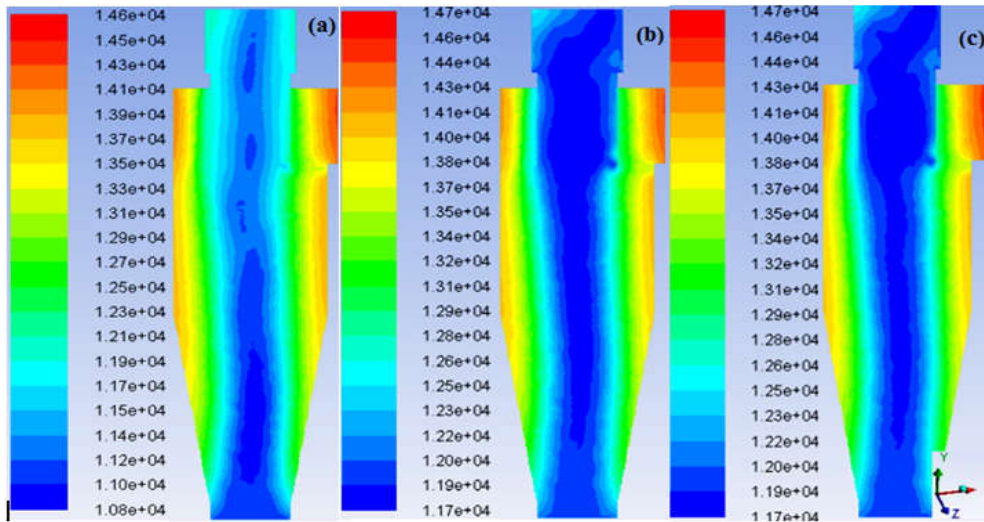
Fig. 5. Contours of static pressure (Pa) at PE100, BL3 and EX5 in a, b and c 3D maps respectively

3.6.2 Pressure Drop in the Double-cyclone

The pressure drops are calculated by CFD simulations in the applied carrier gas flow rates for three polymeric grades. Comparison between the experimental and the simulated results are shown in Fig. 6. However, this comparison reflects the effect of using the RNG k-ε as a turbulence model to simulate the considered double-cyclones.

3.6.3 Turbulence Parameters in the Double-cyclone

Figs. 7 and 8 show a 3D plot of the predicted turbulent dissipation rate and turbulent kinetic energy profiles of the tested gas flow rates. In the model, based on operating conditions and particle specifications, various applied flow rates create turbulence eddy dissipation and turbulence energy for the double-cyclone in various polymeric grades; this indicates the effects of turbulent flow on the particles. A growth in the turbulence kinetic energy happens at the bottom of the cyclone where inner vortex is started. Turbulence energy is higher in PE100 particles, which have greater value in

nitrogen flow rate. These results indicate a direct correlation between the nitrogen flow and the turbulence parameters in which the rise of them can lead to the escape of particles to inner vortex and the reduction of the efficiency of cyclone separation.
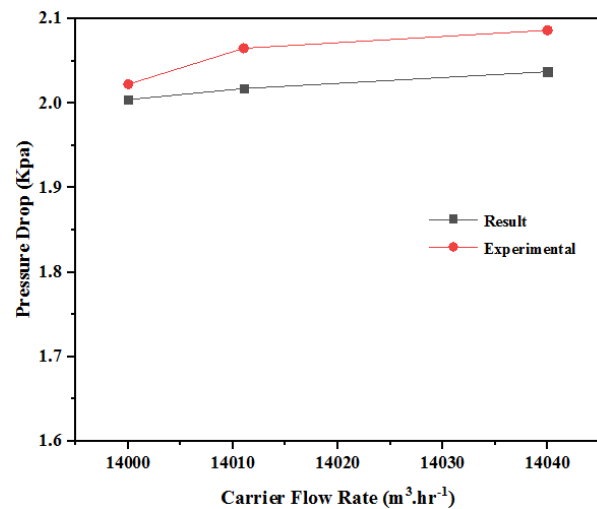
Fig. 6: Pressure drop 2D maps at various HDPE grades of EX5, BL3 and PE100 by operating N_2 flow rates
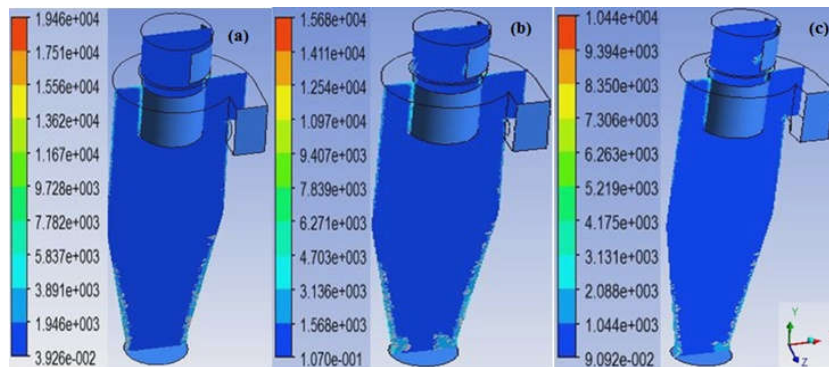
Fig. 7: Contours of turbulence eddy dissipation (m^2s^{-3}) at PE100, BL3 and EX5 in a, b and c 3D maps, respectively
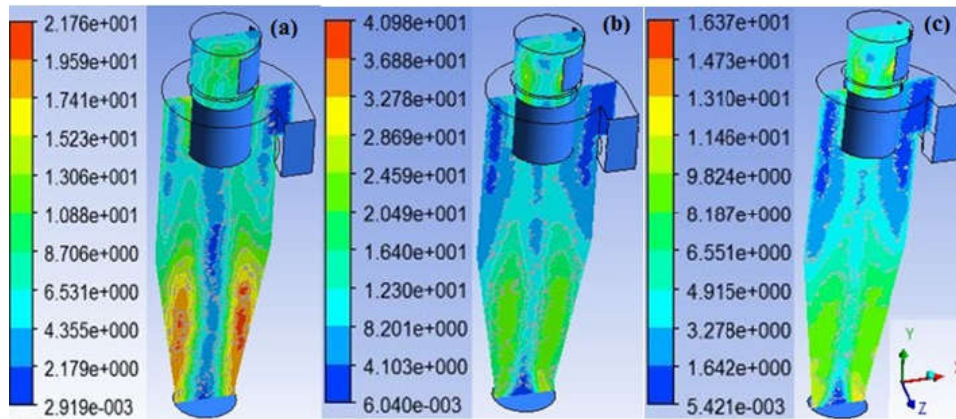
Fig. 8: Contours of turbulence kinetic energy (J kg^{-1}) at PE100, BL3 and EX5 in a, b and c 3D maps, respectively

4. Results and Discussion

The industrial-CFD investigation of the double-cyclone as a complementary unit in the HDPE fluid bed drying confirms that three HDPE grades (PE100, BL3 and EX5) with different densities and PSDs require various nitrogen flow rates to create an appropriate hydrodynamic behavior in the bed. Obtained pressure drops as stable values in PDI-2 show a decrease in these variables for PE100, BL3, and EX5 respectively. PSD curves of HDPE grades, according to Table 2, is shown in Fig. 9. As it can be seen, PE100 particles are coarse powders among the rest of the employed grades like BL3 and EX5. PE100 grades with larger diameters have a greater terminal velocity leading to accumulation of these particles in the bed. Consequently, by checking the PDI-2, it is revealed that PE100 as bigger particles make higher pressure drop in the bed of the dryer. The most important role of the HDPE fluid bed dryer is drying the wet powders to decline the moisture content to 0.1%. Tables 3 to 5 show the volatile contents of three mentioned grades as 0.04%, 0.06%, and 0.07% respectively. it is shown that it is lower than the required value of 0.1% for the final moisture content in the product. These conditions reveal the positive effect of the carrier gas flow rate, which has been adjusted for preparing the dry powders with an acceptable quality.

It is known that the bubbling fluidized bed like our drying system includes two sections, namely a dense phase and a lean one. The dry gas enters the lean phase as a freeboard section after passing through the powders bed. It carries fine particles with a terminal velocity which is lower than the operating gas velocity. This represents the elutriation as a common phenomenon [3, 6-8]. Therefore, the gas stream of the system is the carrier of the dispersed HDPE particles due to the elutriation phenomenon. Particles, which are elutriated by the fluidized gas stream are known as fine particles [7, 8]. The double-cyclones as gas-cleaning systems are used to separate fine particles (dusts) from the exit gas stream prior to discharging in various areas such as distributor plates and the scrubbing tower [3, 6].

Hence, the suitable performance of the cyclone in the drying system affects the de-dusting process. According to Tables 6 and 7, dust content measurements and energy consumption rates show the differences between the proper and unacceptable conditions through the comparison of their values as seen in Figs. 10 and 11.
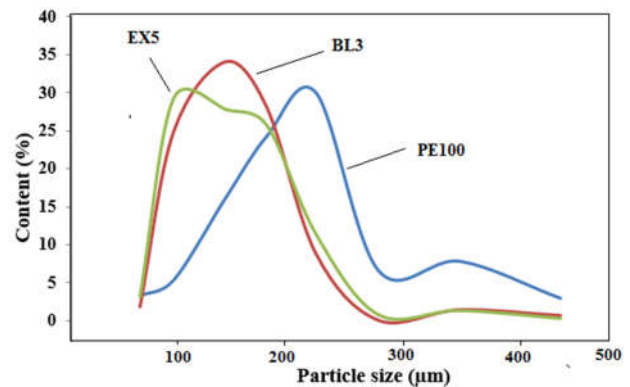
Fig. 9: Compared PSDs of three HDPE grades of PE100, BL3, and EX5 respectively
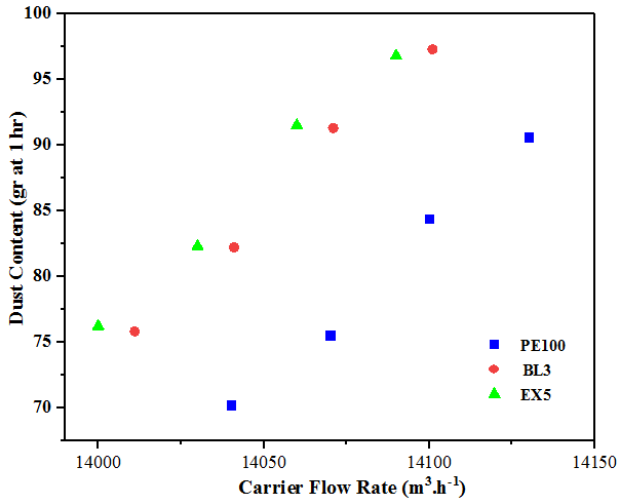
Fig. 10: HDPE dust contents in S.C-2 versus the gas flow rates for three grades of PE100, BL3 and EX5
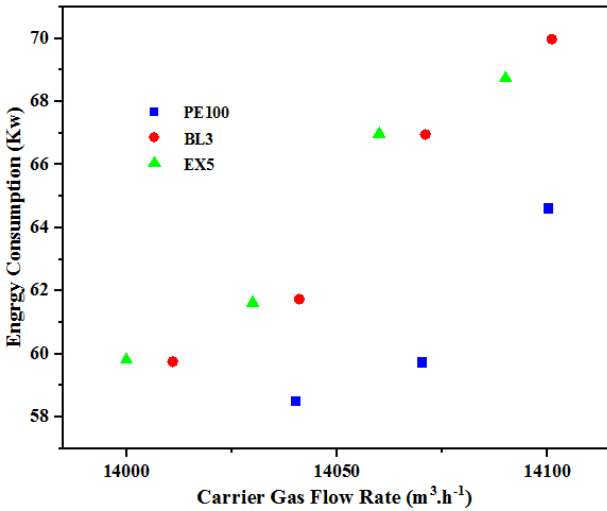
Fig. 11: Energy consumption values versus the gas flow rates for three grades of PE100, BL3 and EX5

Clearly, the appropriate gas flow rates, with the resulted cyclone pressure drops of 2.037, 2.017 and 2.004 kpa in PDI-3, as listed in Tables 3 to 5, create the minimum escaping rate of entrained particles from the cyclones, as shown in Table 6. These low rates of escape affect the electrical energy consumptions and yield an optimized consumption in the blowers after the cyclones. Comparison of Figs. 10 and 11 shows that finer particles like BL3 and EX5 have higher rate of escaped powders and higher energy consumption in the blowers.

According to the Fig. 2, particles enter the tangential inlet in the pattern of the outer vortex. The principle of the separation is the drag force, and the centrifugal forces mainly affect particle motion [20]. Thus, the present CFD model is accurate to predict the trajectory in a discrete phase particle by

integrating the force balance on the particle written in a Lagrangian frame. The centrifugal force F_C at radius r is equal to mU_θ^2/rg_c, where m is the mass of the particle and U_θ is its tangential term [6, 32, 64]. According to both centrifugal concept and obtained relations in this paper (Eq. 9 and 12), the inward drag force pushes the particles toward the axial section and balances the outward centrifugal force on the particles in the radial direction. Accordingly, the particles are distributed from the wall toward the axial area of the cyclone by decreasing the particle size. Despite fine particles, the drag force in large particles is clearly less than the centrifugal force, and these particles are pushed to the cyclone wall and are collected. Interestingly, based on the definition of the centrifugal force exerted on the HDPE particles, a large-diameter cyclone has a much lower separation factor at the same velocity. Therefore, the cyclones in a double-shape geometry with a smaller diameter in this work, compared with the single-cyclones with a large-diameter, have an appropriate separation efficiency, which affects HDPE drying performance.

As stated before, the main contribution to about 80% of the pressure drop is considered to be pressure loss inside the cyclone due to energy dissipation by the viscous stress of the turbulent rotational flow [41]. The remaining 20% of pressure drop is caused by the contraction of the fluid flow at the outlet, by the expansion at the inlet, and by the fluid friction on the cyclone wall surface. The general performance of the equipment is calculated through the static pressure drop between input and output using the following efficiency expression [33, 35, 61, 65, 66]:

$$\Delta P_C = \xi_c \frac{\rho_g V_i^2}{2} \qquad (16)$$

The cyclone pressure drop (ΔP_C) is proportional to square of the velocity (V_i^2), resistance coefficient (ξ_c), and gas density (ρ_g). Euler number (E_u) for the cyclone is defined according to Eq. (17) [67]:

$$E_u = \frac{\Delta P_C}{\frac{1}{2}\rho_g V_i^2} \qquad (17)$$

By using the operational parameters in the CFD simulation, the calculated values of pressure drop are close to the industrial results, as shown in Fig. 6. Accordingly, the RNG k-ε turbulence model yields a reasonably accurate prediction. Hence, due to

memory and CPU limitations, this model is preferred, as the RNG k-ε model is developed from the Standard k-ε model for vortex flows [46, 64]. Because of these advantages, pressure field, pressure drop, and turbulence parameters, as CFD results, will be able to represent the performance of the double-cyclone in the drying system clearly.

Based on previous studies, the performance of the single cyclone can be reported through the pressure drop and cut point diameter (corresponding to separation efficiency of 50% in a partition curve) [68]. For instance, Safikhani et al. showed the reduction of the cut point by increasing the pressure drop in their experiments [69]. Furthermore, Elsayed et al. investigated the effect of geometrical parameters on single cyclone performance in the optimization of cyclone geometry. They proved a superior performance of their new design compared with Stairmand's design [70]. In this research, in addition to considering the suitable design of the cyclones (double-cyclone) and the role of the pressure drop in the separation of the dusts, our innovations include the analysis of energy consumption to improve the performance of the double-cyclone and drying process. Secondly, this work shows the improved performance of HDPE drying process and cyclones by reasonable correlations between the carrier gas flow rates, HDPE types (with different PSDs and densities), the pressure drops of the fluid bed, and the pressure drops of the double-cyclone which is confirmed through industrial-CFD results and optimized energy consumption in the system. In energy analysis, as shown in Figs. 10 and 11, it is obvious that the increment of gas flow rates boosts particles escaping from the gas outlet of the cyclone toward distributor plates and scrubbing tower, which increases electrical energy and affects scrubbing tower trays and distributor orifices at the bottom of dryer. Accordingly, Fig. 12 represents the saving content of the energies consumed by the industrial blowers as a result of controlling the proper carrier gas flow rates.
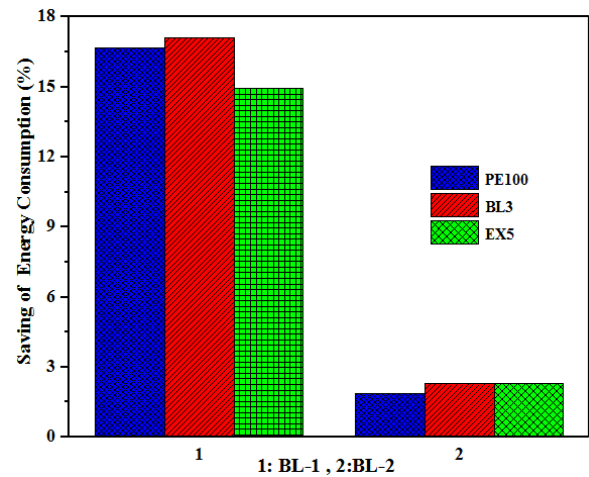
Fig. 12. The values of the energy consumption saving for three grades of PE100, BL3 and EX5

These experiments proved that the fluid bed drying require a certain degree of de-dusting (removal of undesirable fine particles), an operating gas flow rate and an efficient performance in the cyclones. The optimized gas flow rates create low turbulence eddy dissipation and turbulence kinetic energy for the double-cyclone as shown in Figs. 7 and 8 for various grades of PE100, BL3, and EX5. These results indicate that the motion of the fine particles completely depends on the movement of gases. Accordingly, based on the calculated CFD contours in Figs. 7, 8 and the experimental results in Table 6, all particulate escape phenomena such as the short-circuit flow, the re-entrainment, and the drag force towards the inner vortex section, which are caused by the turbulent flow, are relatively weak.

5. Conclusions

In HDPE fluidized bed drying, the performance of the dryer system mainly depends on the particles' behaviors and flow patterns in the dryer, which affect double-cyclones as effective equipment. Navier-Stokes equations with ANSYS Fluent 15.0 in the Euelerian-Lagrangian framework by RNG k-ε turbulence model are used as a mathematical method in CFD simulation. CFD model is applied to characterize cyclone pressure field, pressure drop, and turbulence parameters which helped evaluate the industrial data. Industrial-CFD results show the optimized carrier gas flow rates of 14040, 14011 and 14000 m^3hr^{-1} for PE100, BL3, and EX5 respectively. These nitrogen flow rates create an

optimal hydrodynamic regime without collapse and carryover phenomena in the fluid bed system. In the cyclones, low turbulence eddy dissipation and turbulence kinetic energy provide the minimum rate of the elutriated particles toward the gas outlet. Accordingly, the controlled nitrogen consumptions are obtained as a source of thermal energy in the process. Additionally, resulted regime in the dryer affects the efficient use of the immersed heat exchangers as th other source of energy for drying wet particles. Dry HDPE powders with 0.04%, 0.06% and 0.07% moisture, as the best final quality, were obtained. The de-dusting process is efficiently accomplished as a result of an improved

performance of the cyclones. The double-cyclones in this experiment create the minimum escaped contents of 70.2, 75.8 and 76.2 gr in 1 hr for the distributor section and 69.3, 75.3, 75.9 gr in 1 hr for the scrubbing tower. These rates of escape in the HDPE dusts provide an optimized electrical energy consumption including 58.52, 59.75 and 59.81 kw in the first blower and 99.27, 98.66 and 98.04 in the second blower after the cyclones.

Acknowledgment

Nomenclatures

BL	gas blower
BL3	HDPE blow molding grade
BW	rotary valve
CFD	computational fluid dynamic
C_D	drag coefficient
CY	cyclone
d	particle diameter (m)
$\overline{d}$	mean diameter (m)
EX5	HDPE blown films grade
E_u	Euler number
ΔP_C	pressure drop of cyclone (Pa)
F_C	centrifugal force (N)
F_D	total drag force (N)
FI	flow rate indicator ($m^3.hr^{-1}$)
G_k	generation of turbulent kinetic energy
g	gravity acceleration ($m.s^{-2}$)
HDPE	high-density polyethylene
HX	normal hexane
k	turbulent kinetic energy ($m^2.s^{-2}$)
n	spread parameter
PDI	pressure differential indicator (Pa)
PE100	HDPE pipes grade
PI	pressure indicator (Pa)
PSD	particle size distribution
p	fluid pressure (Pa)
R	effect of swirl
Re	Reynolds number

r	radius of cyclone body (m)
TI	temperature indicator (˚C)
t	time (s)
U_θ	tangential velocity ($m.s^{-1}$)
u	fluid velocity ($m.s^{-1}$)
u_p, v_p, w_p	particle velocity ($m.s^{-1}$)
V_i	inlet velocity of cyclone ($m.s^{-1}$)
x	coordinate system
Y_d	mass fraction of particles
ZN	Ziegler-Natta catalyst

Greek symbol

ε	dissipation rate of turbulent kinetic energy (m^2s^{-3})
μ	fluid viscosity (Pa.s)
μ_{eff}	effective viscosity (Pa.s)
μ_g	gas viscosity (Pa.s)
μ_l	liquid viscosity (Pa.s)
μ_t	turbulent viscosity (Pa.s)
ξ_c	resistance coefficient
ρ	fluid density ($kg.m^{-3}$)
ρ_{Bp}	particle bulk density ($kg.m^{-3}$)
ρ_g	gas density ($kg.m^{-3}$)
ρ_l	hexane density ($kg.m^{-3}$)
ρ_p	dry particle density ($kg.m^{-3}$)
τ	Reynolds stress tensor ($N.m^{-2}$)

Subscript

i,j,k	components in the Cartesian coordinate system

References
[1] Rhodes, M.J., "*Introduction to Particle Technology*", John Wiley & Sons, 2008.

[2] Groenewold, H. and Tsotsas, E., "*Drying in Fluidized Beds with Immersed Heating Elements*", Chem. Eng. Sci., Vol. 62, pp. 481-502, 2007.

[3] Mujumdar, A.S., "*Handbook of industrial drying*", CRC press, 2014.

[4] Harichandan, A.B. and Shamim, T., "*CFD Analysis of Bubble Hydrodynamics in a Fuel Reactor for a Hydrogen-Fueled Chemical Looping Combustion System*", Energy. Convers. Manage., Vol. 86, pp. 1010-1022, 2014.

[5] Luo, S., Xiao, B., Hu, Z., Liu, S. and He, M., "*Experimental Study on Combustion of Biomass Micron Fuel (BMF) in Cyclone Furnace*", Energy. Convers. Manage., Vol. 51, pp. 2098-2102, 2010.

[6] Alavi, S.R. and Lay, E.N., "*Industrial Challenges of HDPE Fluid Bed Drying in Different Grades. QUID: Investigación, Cienciay Tecnología*, pp. 555-566, 2017.

[7] Han, Y.-L., Chyang, C.-S., Hsiao, W.-M. and Lo, K.-C., "*Effect of Fines Hold-up in the Freeboard on Elutriation from a Fluidized Bed*", J. Taiwan. Inst. Chem. Eng., Vol. 42, pp. 120-123, 2011.

[8] Chang, Y.-M., Chou, C.-M., Su, K.-T., Hung, C.-Y. and Wu, C.-H., "*Elutriation Characteristics of Fine Particles from Bubbling Fluidized Bed Incineration for Sludge Cake Treatment*", Waste. manage., Vol. 25, pp. 249-263, 2005.

[9] Altmeyer, S., Mathieu, V., Jullemier, S., Contal, P., Midoux, N., Rode, S. and et al., "*Comparison of Different Models of Cyclone Prediction Performance for Various Operating Conditions Using a General Software*", Chem. Eng. Process. Process Inten., Vol. 43, pp. 511-522, 2004.

[10] Van't Land, C., "*Drying in the process industry*", John Wiley & Sons, 2011.

[11] Winfield, D., Cross, M., Croft, N., Paddison, D. and Craig, I., "*Performance Comparison of a Single and Triple Tangential Inlet Gas Separation Cyclone: A CFD Study*", Powder. Technol., Vol. 235, pp. 520-531 2013.

[12] Misiulia, D., Elsayed, K. and Andersson, A.G., "*Geometry optimization of a deswirler for cyclone separator in terms of pressure drop using CFD and artificial neural network*", Sep. Purif. Technol., Vol. 185, pp. 10-23, 2017.

[13] Liu, F., Chen, J., Zhang, A., Wang, X. and Dong, T., "*Performance and flow behavior of four identical parallel cyclones*", Sep. Purif. Technol., Vol. 134, pp. 147-157, 2014.

[14] Rosin, P., Rammler, E. and Intelmann, W., "*Grundlagen und grenzen der zyklonentstaubung. VDI Zeitschrift*", Vol. 76, pp. 433-437, 1932.

[15] Barth, W., "*Design and Layout of the Cyclone Separator on the Basis of New Investigations*", Brenn Warme Kraft., Vol. 8, pp. 9, 1956.

[16] Dietz, P., "*Collection Efficiency of Cyclone Separators*", AIChE. J., Vol. 27, pp. 888-892, 1981.

[17] Mothes, H. and Löffler, F., "*Prediction of Particle Removal in Cyclone Separators*", Int Chem Eng., Vol. 28, pp. 231-240, 1988.

[18] Dirgo, J. and Leith, D., "*Performance of Theoretically Optimised Cyclones*", Filtr. Sep., Vol. 22, pp. 119-125, 1985.

[19] Leith, D., "*The Collection Efficiency of Cyclone Type Particle Collectors-a New Theoretical Approach*", AIChE Symp Ser., pp. 196-206, 1972.

[20] Song, C., Pei, B., Jiang, M., Wang, B., Xu, D. and Chen, Y., "Numerical Analysis of Forces Exerted on Particles in Cyclone Separators", Powder Technol., vol. 294, pp. 437-448, 2016.

[21] Ter Linden, A., "*Investigations into Cyclone Dust Collectors, Proce*ss", Inst. Mech. Eng., Vol. 160, pp. 233-251, 1949.

[22] Hoekstra, A.J., "*Gas Flow Field and Collection Efficiency of Cyclone Separators*", 2000.

[23] Smith, J., "*An Experimental Study of the Vortex in the Cyclone Separator*", ASME J Basic Eng., Vol. 84, pp. 602-608, 1962.

[24] Solero, G. and Coghe, A., "*Experimental Fluid Dynamic Characterization of a Cyclone Chamber*", Exp. Therm. Fluid. Sci., Vol. 27, pp. 87-96, 2002.

[25] Syred, N., "*A Review of Oscillation Mechanisms and the Role of the Precessing Vortex Core (PVC) in Swirl Combustion Systems*", Progress Energy. Combust. Sci., Vol. 32, pp. 93-161, 2006.

[26] Cortes, C. and Gil, A., "*Modeling the Gas and Particle Flow Inside Cyclone Separators*", Progress Energy. Comb. Sci., Vol. 33, pp. 409-452, 2007.

[27] Su, Y. and Mao, Y., "*Experimental Study on the Gas–Solid Suspension Flow in a Square Cyclone Separator*", Chem. Eng. J., Vol. 121, pp. 51-58, 2006.

[28] Chan, C., Seville, J., Fan, X., Dewil, R. and Baeyens, J., "*CFB Cyclones: Pressure Drop and Particle Motion, Viewed by Positron Emission Particle Tracking*", 2008.

[29] Li, S., Yang, H., Zhang, H., Yang, S., Lu, J. and Yue, G., "*Measurements of Solid Concentration and Particle Velocity Distributions Near the Wall of a Cyclone*", Chem. Eng. J., Vol. 150, pp. 168-173, 2009.

[30] Cocco, R., Karri, S.R. and Knowlton, T., "*Introduction to fluidization*", Chem. Eng. Progress, Vol. 110, pp. 21-29, 2014.

[31] Drake, J.B., "*Hydrodynamic Characterization of 3D Fluidized Beds Using Noninvasive Techniques*", Iowa State University, 2011.

[32] Lay, E.N., Razavi Alavi, S.A., Afzali, K. and Alizadeh Makhmali, A.H., "*Investigation of Effective Operational Parameters on an Industrial Double-Cyclone of HDPE Fluidized Bed Drying*", The 9th Int. Chem. Eng. Congress Exhibition, IRAN, 2015.

[33] Safikhani, H. and Mehrabian, P., "*Numerical Study of Flow Field in New Cyclone Separators*", Adv. Powder. Technol., Vol. 27, pp. 379-387, 2016.

[34] Lee, J.W., Yang, H.J. and Lee, D.Y., "*Effect of the Cylinder Shape of a Long-Coned Cyclone on the Stable Flow-Field Establishment*", Powder Technol., Vol. 165, pp. 30-38, 2006.

[35] Gimbun, J., Chuah, T., Fakhru'l-Razi, A. and Choong, T.S., "*The Influence of Temperature and Inlet Velocity on Cyclone Pressure Drop: a CFD Study*", Chem. Eng. Process. Process Inten., Vol. 44, pp. 7-12, 2005.

[36] Su, M., Zhao, H. and Ma, J., "*Computational Fluid Dynamics Simulation for Chemical Looping Combustion of Coal in a Dual Circulation Fluidized Bed*", Energy. Convers. Manage., Vol. 105, pp. 1-12, 2015.

[37] A. Kasaeian, A.R. Mahmoudi, F.R. Astaraei, A. Hejab, "*3D Simulation of Solar Chimney Power Plant Considering Turbine Blades*", Energy. Convers. Manage., Vol. 147, pp. 55-65, 2017.

[38] A. Fluent. 12.0 Theory Guide. Ansys Inc. 5, 2009.

[39] A. Fluent. Fluent theory guide. SAS IP, Inc, Canonsburg, PA., 2010.

[40] Ghasemian, M., Ashrafi, Z.N. and Sedaghat, A., "*A Review on Computational Fluid Dynamic Simulation Techniques for Darrieus Vertical Axis Wind Turbines*", Energy. Convers. Manage., Vol. 149, pp. 87-100, 2017.

[41] Jayaraju, S.T., "*Study of the Air Flow and Aerosol Transport in the Human Upper Airways Using LES and DES Methodologies*", Mech. Eng., pp. 196, 2009.

[42] Stairmand, C.J., "*The Design and Performance of Cyclone Separators*", Trans Inst Chem Engrs., Vol. 29, pp. 356-362, 1951.

[43] Shephered, C. and Lapple, C., "*Flow Pattern and Pressure Drop in Cyclone dust Collectors*", Ind. Eng. Chem., Vol. 31, pp. 972-984, 1939.

[44] A. Ogawa, "*Separation of Particles from air and Gases*", 1984.

[45] Ficici, F., Ari, V. and Kapsiz, M., "*The Effects of Vortex Finder on the Pressure Drop in Cyclone Separators*", Int. J. Physical. Sci., Vol. 5, pp. 804-813, 2010.

[46] Bernardo, S., Mori, M., Peres, A. and Dionisio, R., "*3-D Computational Fluid Dynamics for Gas and Gas-Particle Flows in a Cyclone with Different Inlet Section Angles*", Powder Technol., Vol. 162, pp. 190-200, 2006.

[47] Chuah, T., Gimbun, J. and Choong, T.S., "*A CFD Study of the Effect of Cone Dimensions on Sampling Aerocyclones Performance and Hydrodynamics*", Powder Technol., Vol. 162, pp. 126-132, 2006.

[48] Dyakowski, T. and Williams, R., "*Modelling Turbulent Flow within a Small-Diameter Hydrocyclone*", Chem. Eng. Sci., Vol. 48, pp. 1143-1152, 1993.

[49] Griffiths, W. and Boysan, F., "*Computational Fluid Dynamics (CFD) and Empirical Modelling of the Performance of a Number of Cyclone Samplers*", J. Aerosol Sci., Vol. 27, pp. 281-304, 1996.

[50] Peng, W., Hoffmann, A., Boot, P., Udding, A., Dries, H., Ekker, A. and et al., "*Flow Pattern in Reverse-Flow Centrifugal Separators*", Powder Technol., Vol. 127, pp. 212-222, 2002.

[51] Xiang, R. and Lee, K., "*Numerical Study of Flow Field in Cyclones of Different Height*", Chem. Eng. Process. Process Inten., Vol. 44, pp. 877-883, 2005.

[52] Zhou, L. and Soo, S., "*Gas—Solid Flow and Collection of Solids in a Cyclone Separator*", Powder Technol., Vol. 63, pp. 45-53, 1990.

[53] Houben, J., Weiss, C., Brunnmair, E. and Pirker, S., "*CFD Simulations of Pressure Drop and Velocity Field in a Cyclone Separator with Central Vortex Stabilization Rod*", J. Appl. Fluid. Mech., Vol. 9, 2016.

[54] Huang, A.-N., Ito, K., Fukasawa, T., Yoshida, H., Kuo, H.-P. and Fukui, K., "*Classification Performance Analysis of a Novel Cyclone with a Slit on the Conical part by CFD Simulation*", Sep. Purif. Technol., Vol. 190, pp. 25-32, 2018.

[55] Thompson, J.F., Warsi, Z.U. and Mastin, C.W., "*Numerical Grid Generation: Foundations and Applications*", North-holland Amsterdam, 1985.

[56] Ansys. I., CFD. ICEM CFD theory guide, Ansys inc. 2015.

[57] Zhao, B., Su, Y. and Zhang, J., "*Simulation of Gas Flow Pattern and Separation Efficiency in Cyclone with Conventional Single and Spiral Double Inlet Configuration*", Chem. Eng. Research. Design., Vol. 84, pp. 1158-1165, 2006.

[58] Jiao, J., Zheng, Y. Sun, G. and Wang, J., "*Study of the Separation Efficiency and the Flow Field of a Dynamic Cyclone*", Sep. Purif. Technol., Vol. 49, pp. 157-166, 2006.

[59] Orszag, S.A., "*Renormalisation Group Modelling and Turbulence Simulations. Near-wall Turbulent Flows*", 1993.

[60] Choudhury, D., "*Introduction to the Renormalization Group Method and Turbulence Modeling. Fluent Incorporated*, 1993.

[61] Morsi, S. and Alexander, A., "*An Investigation of Particle Trajectories in Two-Phase Flow Systems*", J. Fluid. Mech., Vol. 55, pp. 193-208, 1972.

[62] Curtis, J.S. and Van Wachem, B., "*Modeling Particle-Laden Flows: A research outlook*", AIChE. J., Vol. 50, pp. 2638-2645, 2004.

[63] Ferziger, J.H. and Peric, M., "*Computational Methods for Fluid Dynamics*", Springer Science & Business Media, 2012.

[64] Wang, B., Xu, D., Chu, K. and Yu, A., "*Numerical Study of Gas–Solid Flow in a Cyclone Separator*", Appl. Math. Modelling, Vol. 30, pp. 1326-1342, 2006.

[65] McCabe, W.L., Smith, J.C. and Harriott, P., "*Unit Operations of Chemical Engineering*", McGraw-Hill, New York, 1993.

[66] Sgrott, O.L., Noriler, D., Wiggers, V.R. and Meier, H.F., "*Cyclone Optimization by COMPLEX Method and CFD Simulation*", Powder Technol., Vol. 277, pp. 11-21, 2015.

[67] Li, Q., Xu, W., Wang, J. and Jin, Y., "*Performance Evaluation of a New Cyclone Separator–Part I Experimental Results*", Sep. Purif. Technol., Vol. 141, pp. 53-58, 2015.

[68] Ghodrat, M., Kuang, S., Yu, A., Vince, A., Barnett, G. and Barnett, P., "*Computational Study of the Multiphase Flow and Performance of Hydrocyclones: Effects of Cyclone Size and Spigot Diameter*", Ind. Eng. Chem. Research., Vol. 52, pp. 16019-16031, 2013.

[69] Safikhani, H., Hajiloo, A. and Ranjbar, M., "*Modeling and Multi-Objective Optimization of Cyclone Separators Using CFD and Genetic Algorithms*", Comp. Chem. Eng., Vol. 35, pp. 1064-1071, 2011.

[70] Elsayed, K. and Lacor, C., "*CFD Modeling and Multi-Objective Optimization of Cyclone Geometry Using Desirability Function, Artificial Neural Networks and Genetic Algorithms*", Appl. Math. Modelling., Vol. 37, pp. 5680-5704, 2013.